X-chromosome upregulation is dynamically linked to the X-inactivation state

Antonio Lentini[1], Martin Enge[2], Qiaolin Deng[3] and Björn Reinius[1]*

[1]Department of Medical Biochemistry and Biophysics, Karolinska Institutet, Stockholm, Sweden.
[2]Department of Oncology and Pathology, Karolinska Institutet, Stockholm, Sweden.
[3]Department of Physiology and Pharmacology, Karolinska Institutet, Stockholm, Sweden.
*Correspondence to: bjorn.reinius@ki.se

One sentence summary: Expression of mammalian X chromosomes is dynamically balanced between both alleles to compensate dosage imbalances.

Keywords: X-chromosome upregulation, X-inactivation, embryo development, dosage compensation, Ohno's hypothesis.

Abstract

The interplay between X-chromosome upregulation (XCU) and X-chromosome inactivation (XCI) to balance allelic expression is poorly understood. Here, we mapped XCU throughout early mouse embryonic development at cellular and allelic resolution, revealing sex- and lineage-specific dynamics along key events in X-chromosome regulation. XCU was linearly proportional to the degree of XCI, indicating that upregulation ensued based on mRNA levels rather than number of active X chromosomes, and was underlain by increased transcriptional burst frequencies. Surprisingly, our data show that the two active X chromosomes in female naïve embryonic stem cells are not hyperactive, which has major implications for reprogramming studies. Together, our results demonstrate unappreciated flexibility of XCU, and we propose a general model for allelic dosage balance, applicable for wider mechanisms of transcriptional regulation.

Main

In therian mammals, the X chromosome is present as two copies in females and one in males. Correct balance of gene dosage is vital for homeostasis and normal cell function and two major, X-chromosome-wide, mechanisms ensure balanced genomic expression. XCI silences one X allele in females, equalizing expression between the sexes, and XCU increases X-linked expression to resolve dosage imbalance against autosomal gene networks [reviewed in (*1*)]. Although the existence of XCU is well supported by relative measurements between X and autosomes (*2*–*6*), the dynamics of its establishment and maintenance remain elusive (*6*–*8*). Such unraveling would require quantitative gene expression measurements at cellular and allelic resolution, only recently made possible by allele-sensitive single-cell RNA-seq (scRNA-seq), and analytical disentanglement of other allelic processes at cellular level such as stochastic allelic expression and random XCI (rXCI) (*9*). Here, we have mapped the XCU process in mouse at allelic and cellular resolution throughout its establishment *in vitro* and *in vivo*, revealing fundamental features and a surprising plasticity in this process, and we provide a unified model of this chromosome-wide mode of gene regulation.

We started by culturing naïve male and female mouse embryonic stem cells (mESCs) derived from F1 hybrids of strains C57BL/6J and CAST/EiJ (hereafter C57 and CAST, respectively), and we subsequently differentiated female mESCs into epiblast stem cells (EpiSCs) to induce rXCI (**Fig. 1A, Methods**). We harvested naïve mESCs and EpiSCs throughout differentiation (day 1, 2, 4 and 7) and subjected cells to scRNA-seq using the recently published Smart-seq3 method (*10*) (**Fig. 1A, Methods**), allowing sensitive allele- and molecule-level analysis at cellular resolution (**fig. S1A**). Differentiation induced distinct expression changes accompanied by loss of pluripotency factors (*e.g. Sox2* & *Nanog*) and induction of lineage-specific factors (*e.g. Fgf5* & *Krt18*) (**Fig. 1B-C**, **fig. S1B** & **Table S1**) as well as enrichment for associated pathways (**fig. S1C** & **Table S1**). *Xist* induction was detected already by differentiation day 1 (**fig. S1D**), accompanied by the transition from biallelic to monoallelic X-chromosome expression (**Fig. 1D**) and signifying successful rXCI. To investigate XCU, we stratified female cells based on rXCI status into active (XaXa) and inactive (XaXi) state inferred from allelic expression (**Fig. 1D, Methods**) and calculated X-chromosome expression per cell and allele. Intriguingly, we detected chromosome-wide upregulation of the active X allele in female cells with established rXCI and in male mESCs, but lack thereof in cells of XaXa state (**Fig. 1E-F**). We calculated total expression of the different X states and observed the combined output of two moderately active XaXa alleles to be higher than that of a single hyperactive allele ($FDR_{TPM} \leq 4.35 \times 10^{-34}$, $FDR_{UMI} \leq 6.86 \times 10^{-5}$, Mann-Whitney *U* test; **Fig. 1G-H and fig. S1E**). Furthermore, gene-wise fold-changes of the active allele transitioning from XaXa into XaXi state (**Fig. 1I**, shown for both C57 and CAST alleles) demonstrated distinct X-upregulation, but with fold-change below two (median $X_{C57} = 1.62$, $P_{C57} = 1.41 \times 10^{-40}$ and median $X_{CAST} = 1.67$, $P_{CAST} = 5.72 \times 10^{-48}$, Wilcoxon signed-rank test). This is important as it alters the notion that XCI acts on an hyperactive XaXa state (*3*, *5*, *11*). It furthermore directly explains why measured female-to-male X-chromosome expression fold-change in naïve ESC tend to be less than two-fold (*5*, *11*), and is consistent with the notion that expression dosage of two active X alleles blocks or delays differentiation of mESCs (*12*).

Previous studies have linked XCU to increased transcriptional initiation (*3*, *13*, *14*) and bursting (*15*). We inferred parameters of transcriptional burst kinetics using both molecule- (UMI) and read-count (TPM) data (**Methods**), revealing moderate and balanced burst frequencies for the two XaXa alleles whereas all states of a singly active X allele displayed markedly increased burst frequency ($FDR_{TPM} \leq 3.97 \times 10^{-10}$, $FDR_{UMI} \leq 5.68 \times 10^{-03}$, Mann-Whitney *U* test; **Fig. 1J**). Burst sizes were not increased but remained largely constant (FDR ≥ 0.08, **Fig. 1J**), consistent with our previous findings that XCU is driven by increased transcriptional burst frequencies (*15*).

Naïve mESCs are derived from, and mimic, the inner cell mass (ICM) of preimplantation stage embryos. To obtain an allelic map of XCU dynamics throughout the *in vivo* pre- and peri-implantation development, we leveraged the large allele-level scRNA-seq datasets we recently generated for the same F1 breed across early murine embryogenesis (*16*–*18*), encompassing the main events of XCI (*1*) (**Fig. 2A**). We calculated allelic X-chromosome expression and observed initiation of XCU at the 4-cell stage in males, *i.e*. around completion of zygotic genome activation (ZGA) (**Fig. 2B**), whereas female cells displayed balanced allelic expression until the 8-to-16-cell stage (**Fig. 2B**) coinciding with imprinted XCI (iXCI). This implies that XCU is initiated in concert with unbalanced chromosomal dosage in a sex-specific manner. We observed maintained XCU throughout preimplantation blastocyst development in both sexes (**Fig. 2B**). To investigate XCU in the emerging lineages in this window of development, we first performed graph-based clustering of blastocyst cells into ICM, trophectoderm (TE) and two immature clusters, followed by hierarchical clustering of ICM into epiblast (EPI) and primitive endoderm (PrE) based on known lineage markers (**fig. S2A-B, Methods**). This showed XCU to be present in all lineages of the late blastocyst, including EPI cells prior to X-chromosome reactivation (XCR) (**fig. S2C**), again suggesting that XCU is regulated based on active X alleles. Indeed, during post-implantation development (E5.5-6.5), male cells (independent of lineage) and female cells of extraembryonic lineages (visceral endoderm, VE; extraembryonic ectoderm, ExE) retained XCU along with iXCI across all timepoints (**Fig. 2C**). As expected, female E5.5 EPI cells, residing in reactivated XaXa state, showed X-linked expression close to autosomal levels for each allele (**Fig. 2C**), importantly demonstrating erasure of XCU *in vivo*. This was followed by a second wave of XCU in cells where rXCI was either underway or completed (E6.0–6.5) (**Fig. 2C**). As rXCI is an asynchronous process (*16*, *17*), we stratified and analyzed EPI cells based on rXCI status which verified that cells of XaXa state expressed each X allele at moderate level, similar to autosomes (**Fig. 2D**), consistent with our *in vitro* findings (**Fig. 1**). Intriguingly, XCU displayed gradual chromosome-wide re-establishment along with rXCI establishment (**Fig. 2D**-**E**), suggesting that XCU is not a trigger-like mechanism but a dynamic, tuning-like, process. To control for effects related to differentiation, we inferred pseudotime differentiation trajectories for each lineage (**fig. S2D-E**, **Methods**), demonstrating minimal association with X-linked expression compared to allele usage in linear regression (**fig. S2F**). If allelic X expression dosage is compensated based on output rather than active chromosome copies, such a mechanism would ensure similar mRNA levels regardless of degree of XCI. Indeed, allelic X-linked expression was highly correlated with maternal fractions in EPI cells (adjusted $R^2_{maternal} = 0.80$, $P_{maternal} = 2.92 \times 10^{-69}$, adjusted $R^2_{paternal} = 0.91$, $P_{paternal} = 1.19 \times 10^{-103}$, linear regression; **Fig. 3A & fig. S3A**). Surprisingly, genes escaping XCI showed similar trends to other X-linked genes ($P_{maternal} = 0.62$, $P_{paternal} = 0.71$, Kolmogorov–Smirnov test; **fig. S3A**) which would be unlikely if XCU is independently regulated per gene and allele. Furthermore, variability of iXCI completeness in extraembryonic lineages and pre-implantation stages also followed the trend projected from EPI cells (**Fig. 3A & fig. S3B**), suggesting that the first, iXCI-associated, wave of XCU is achieved by the same mechanism.

Notably, previous studies lacking allelic resolution approximated XCU using X:autosome (X:A) expression ratios (*3*–*6*) for which the tuning-like compensation (XaXi > XaXs > XaXa) would be undetectable. Indeed, X:A ratios were indistinguishable in non-XaXa cells, regardless of sex, lineage and rXCI status (median EPI = 0.85–0.86 (XaXa = 0.98); VE = 0.81–0.93; ExE = 0.86–0.90; **Fig. 3C & fig. S3C-D, Methods**). Interestingly, ancestral X-Y gene pairs were not upregulated in males whereas corresponding X-linked homologs were subject to XCU in females (**fig. S3E-G** & **Table S2**).

Due to caveats with indirect comparisons across chromosomes (*i.e.* X:A ratios), we sought to directly assess the dosage balancing dynamics of XCU. As male cells persistently exhibited XCU past ZGA, we compared male and female Xa alleles along rXCI which indeed revealed that expression of the female Xa allele gradually increased towards male X levels as rXCI progressed (**Fig. 3C & fig. S3H**). We extended this comparison by calculating gene-wise female:male expression ratios at allelic- (Xa) and global level (Xm+Xp) per lineage, embryonic day and rXCI state (**Methods**). This showed that global gene-level expression was balanced in all except XaXa cells whereas female Xa alleles showed progressive upregulation along rXCI (**Fig. 3D**), consistent with balanced mRNA levels between both alleles. The increased relative expression in XaXa cells is in agreement with our *in vitro* results (**Fig. 1H-I**) and was further supported by reanalysis of bulk RNA-seq data (**Methods**) where mESCs of male sex (XY) and female cells lacking one X-chromosome copy (XO) displayed lower X-linked expression compared to XX cells (**Fig. 3E**),

confirming that XCU of one allele does not fully reach the combined XaXa levels.

If XCU tunes expression based on mRNA levels, we expect transcription from the Xa allele to be merely slightly increased in cells with partially established XCI due to residual mRNAs from the other allele. We inferred transcriptional kinetics of XCU *in vivo* and indeed found that burst frequencies on the Xa allele were progressively increased during rXCI establishment (**Fig. 3F**) whereas burst sizes remained similar to autosomal levels upon XCU (**fig. S3I**). Next, we inferred transcriptional kinetics in extraembryonic cells subject to iXCI, also revealing increased burst frequencies for the Xa allele (**Fig. 3F**), again pointing to a unified XCU mechanism in all lineages.

By allele-level mRNA measurements in single cells throughout differentiation *in vitro* and early development *in vivo*, we have provided a unified model of XCU, schematically summarized in **Fig. 4**. We show distinct sex-specific initiation of XCU where X:autosome dosage would otherwise be unbalanced; after completion of ZGA in males, and together with iXCI in females. This is in contrast to previous studies suggesting XCU to be established already in the zygote (*6*) or progressively after the 4-cell stage in both sexes (*7*, *8*) using X:A ratios. These discrepancies are explained by the inability of non-allelic measurements to correctly distinguish XCU in the presence of other allelic processes, such as ZGA and XCI, whereas we directly attribute XCU to the active X allele. Furthermore, we reveal that naïve mESCs cells lack XCU whereas previous studies assumed XCU to be active in these cells (*3*, *5*, *19*), likely explained by the fact that total XaXa expression levels are higher than what is achieved through XCU.

What is the mechanism underlying these XCU dynamics? Our findings are in line with a recently proposed model (*20*) where balance is achieved by local transcription factor concentrations. As XCI is gradually established (*21*), transcription factors shift to the active X allele, increasing transcriptional burst frequencies (*22*) resulting in increased mRNA levels. This would explain why active histone modifications do not scale proportionally with mRNA levels on the hyperactive X allele (*13*, *14*) and why genes that escape XCI are subject to similar dosage balancing as other X-linked genes. Enhancer elements likely play key roles in mediating XCU as they may not only increase local transcription factor concentrations through DNA contacts (*23*) but also regulate transcriptional burst frequencies (*24*) which is a driver of XCU (*15*).

Our findings that XaXa cells lack XCU is in line with balanced X:A dosage in haploid cells (including MII oocytes) and other cells with two active X chromosomes, such as primary oocytes and primordial germ cells (*6*, *25–27*). Two active X chromosomes is considered a hallmark of the naïve female stem cell state and a gold standard in reprogramming studies (*28*). Our model of two moderately active alleles in the XaXa state in contrast to hyperactive female XaXi and male XaY alters the interpretation of X-chromosome expression level measurements for assessment of reprogramming success and naïveness. Furthermore, in light of our current results in mouse, it is plausible that the "dampened" biallelic X-chromosome state reported in human preimplantation development (*29–31*) and human naïve pluripotent stem cells (*32*) might reflect erasure (*33*) of XCU.

Together, this study provides a unified model of XCU and its link to XCI, and evidence for flexible balancing of allelic expression levels to compensate for dosage imbalance of the X chromosome.

References

1. X. Deng, J. B. Berletch, D. K. Nguyen, C. M. Disteche, X chromosome regulation: Diverse patterns in development, tissues and disease. *Nat. Rev. Genet.* **15**, 367–378 (2014).
2. D. A. Adler, E. I. Rugarli, P. A. Lingenfelter, K. Tsuchiya, D. Poslinski, H. D. Liggitt, V. M. Chapman, R. W. Elliott, A. Ballabio, C. M. Disteche, Evidence of evolutionary up-regulation of the single active X chromosome in mammals based on Clc4 expression levels in Mus spretus and Mus musculus. *Proc. Natl. Acad. Sci. U. S. A.* **94**, 9244–9248 (1997).
3. X. Deng, J. B. Hiatt, D. K. Nguyen, S. Ercan, D. Sturgill, L. W. Hillier, F. Schlesinger, C. A. Davis, V. J. Reinke, T. R. Gingeras, J. Shendure, R. H. Waterston, B. Oliver, J. D. Lieb, C. M. Disteche, Evidence for compensatory upregulation of expressed X-linked genes in mammals, Caenorhabditis elegans and Drosophila melanogaster. *Nat. Genet.* **43**, 1179–1185 (2011).
4. V. Gupta, M. Parisi, D. Sturgill, R. Nuttall, M. Doctolero, O. K. Dudko, J. D. Malley, P. S. Eastman, B. Oliver, Global analysis of X-chromosome dosage compensation. *J. Biol.* **5** (2006), doi:10.1186/jbiol30.
5. H. Lin, V. Gupta, M. D. Vermilyea, F. Falciani, J. T. Lee, L. P. O'Neill, B. M. Turner, Dosage compensation in the mouse balances up-regulation and silencing of X-linked genes. *PLoS Biol.* **5**, 2809–2820 (2007).
6. D. K. Nguyen, C. M. Disteche, Dosage compensation of the active X chromosome in mammals. *Nat. Genet*. **38**, 47–53 (2006).
7. M. Borensztein, L. Syx, K. Ancelin, P. Diabangouaya, C. Picard, T. Liu, J. B. Liang, I. Vassilev, R. Galupa, N. Servant, E. Barillot, A. Surani, C. J. Chen, E. Heard, Xist-dependent imprinted X inactivation and the early developmental consequences of its failure. *Nat. Struct. Mol. Biol.* **24**, 226–233 (2017).
8. F. Wang, J. D. Shin, J. M. Shea, J. Yu, A. Bošković, M. Byron, X. Zhu, A. K. Shalek, A. Regev, J. B. Lawrence, E. M. Torres, L. J. Zhu, O. J. Rando, I. Bach, Regulation of X-linked gene expression during early mouse development by Rlim. *eLife*. **5** (2016), doi:10.7554/eLife.19127.
9. B. Reinius, R. Sandberg, Random monoallelic expression of autosomal genes: stochastic transcription and allele-level regulation. *Nat. Rev. Genet.* **16**, 653–664 (2015).
10. M. Hagemann-Jensen, C. Ziegenhain, P. Chen, D. Ramsköld, G.-J. Hendriks, A. J. M. Larsson, O. R. Faridani, R. Sandberg, Single-cell RNA counting at allele and isoform resolution using Smart-seq3. *Nat. Biotechnol.* **38**, 708–714 (2020).
11. H. Lin, J. A. Halsall, P. Antczak, L. P. O'Neill, F. Falciani, B. M. Turner, Relative overexpression of X-linked genes in mouse embryonic stem cells is consistent with Ohno's hypothesis. *Nat. Genet.* **43**, 1169–1170 (2011).

12. E. G. Schulz, J. Meisig, T. Nakamura, I. Okamoto, A. Sieber, C. Picard, M. Borensztein, M. Saitou, N. Blüthgen, E. Heard, The Two Active X Chromosomes in Female ESCs Block Exit from the Pluripotent State by Modulating the ESC Signaling Network. *Cell Stem Cell*. **14**, 203–216 (2014).
13. X. Deng, J. B. Berletch, W. Ma, D. K. Nguyen, J. B. Hiatt, W. S. Noble, J. Shendure, C. M. Disteche, Mammalian X upregulation is associated with enhanced transcription initiation, RNA half-life, and MOF-mediated H4K16 acetylation. *Dev. Cell*. **25**, 55–68 (2013).
14. E. Yildirim, R. I. Sadreyev, S. F. Pinter, J. T. Lee, X-chromosome hyperactivation in mammals via nonlinear relationships between chromatin states and transcription. *Nat. Struct. Mol. Biol.* **19**, 56–62 (2012).
15. A. J. M. Larsson, C. Coucoravas, R. Sandberg, B. Reinius, X-chromosome upregulation is driven by increased burst frequency. *Nat. Struct. Mol. Biol.* **26**, 963–969 (2019).
16. G. Chen, J. P. Schell, J. A. Benitez, S. Petropoulos, M. Yilmaz, B. Reinius, Z. Alekseenko, L. Shi, E. Hedlund, F. Lanner, R. Sandberg, Q. Deng, Single-cell analyses of X Chromosome inactivation dynamics and pluripotency during differentiation. *Genome Res.* **26**, 1342–1354 (2016).
17. S. Cheng, Y. Pei, L. He, G. Peng, B. Reinius, P. P. L. Tam, N. Jing, Q. Deng, Single-Cell RNA-Seq Reveals Cellular Heterogeneity of Pluripotency Transition and X Chromosome Dynamics during Early Mouse Development. *Cell Rep.* **26**, 2593–2607.e3 (2019).
18. Q. Deng, D. Ramsköld, B. Reinius, R. Sandberg, Single-cell RNA-seq reveals dynamic, random monoallelic gene expression in mammalian cells. *Science*. **343**, 193–196 (2014).
19. M. Wang, F. Lin, K. Xing, L. Liu, Random X-chromosome inactivation dynamics in vivo by single-cell RNA sequencing. *BMC Genomics*. **18**, 9–10 (2017).
20. X. Deng, C. M. Disteche, Rapid transcriptional bursts upregulate the X chromosome. *Nat. Struct. Mol. Biol.* **26**, 851–853 (2019).
21. H. Marks, H. H. D. Kerstens, T. S. Barakat, E. Splinter, R. A. M. Dirks, G. van Mierlo, O. Joshi, S. Y. Wang, T. Babak, C. A. Albers, T. Kalkan, A. Smith, A. Jouneau, W. de Laat, J. Gribnau, H. G. Stunnenberg, Dynamics of gene silencing during X inactivation using allele-specific RNA-seq. *Genome Biol.* **16**, 9–10 (2015).
22. I. Brouwer, T. L. Lenstra, Visualizing transcription: key to understanding gene expression dynamics. *Curr. Opin. Chem. Biol.* **51**, 122–129 (2019).
23. R. Cortini, G. J. Filion, Theoretical principles of transcription factor traffic on folded chromatin. *Nat. Commun.* **9**, 9–10 (2018).
24. A. J. M. Larsson, P. Johnsson, M. Hagemann-Jensen, L. Hartmanis, O. R. Faridani, B. Reinius, \AAsa Segerstolpe, C. M. Rivera, B. Ren, R. Sandberg, Genomic encoding of transcriptional burst kinetics. *Nature*. **565**, 251–254 (2019).
25. A. Fukuda, M. Tanino, R. Matoba, A. Umezawa, H. Akutsu, Imbalance between the expression dosages of X-chromosome and autosomal genes in mammalian oocytes. *Sci. Rep.* **5**, 9–10 (2015).
26. X. Li, Z. Hu, X. Yu, C. Zhang, B. Ma, L. He, C. Wei, J. Wu, Dosage compensation in the process of inactivation/reactivation during both germ cell development and early embryogenesis in mouse. *Sci. Rep.* **7** (2017), doi:10.1038/s41598-017-03829-z.
27. M. N. Sangrithi, H. Royo, S. K. Mahadevaiah, O. Ojarikre, L. Bhaw, A. Sesay, A. H. F. M. Peters, M. Stadler, J. M. A. Turner, Non-Canonical and Sexually Dimorphic X Dosage Compensation States in the Mouse and Human Germline. *Dev. Cell*. **40**, 289–301.e3 (2017).
28. S. Augui, E. P. Nora, E. Heard, Regulation of X-chromosome inactivation by the X-inactivation centre. *Nat. Rev. Genet.* **12**, 429–442 (2011).
29. S. Petropoulos, D. Edsgärd, B. Reinius, Q. Deng, S. P. Panula, S. Codeluppi, A. Plaza Reyes, S. Linnarsson, R. Sandberg, F. Lanner, Single-Cell RNA-Seq Reveals Lineage and X Chromosome Dynamics in Human Preimplantation Embryos. *Cell*. **165**, 1012–1026 (2016).
30. F. Zhou, R. Wang, P. Yuan, Y. Ren, Y. Mao, R. Li, Y. Lian, J. Li, L. Wen, L. Yan, J. Qiao, F. Tang, Reconstituting the transcriptome and DNA methylome landscapes of human implantation. *Nature*. **572**, 660–664 (2019).
31. I. Okamoto, A. P. Otte, C. D. Allis, D. Reinberg, E. Heard, Epigenetic dynamics of imprinted X inactivation during early mouse development. *Science*. **303**, 644–649 (2004).
32. A. Sahakyan, R. Kim, C. Chronis, S. Sabri, G. Bonora, T. W. Theunissen, E. Kuoy, J. Langerman, A. T. Clark, R. Jaenisch, K. Plath, Human Naive Pluripotent Stem Cells Model X Chromosome Dampening and X Inactivation. *Cell Stem Cell*. **20**, 87–101 (2017).
33. S. Mandal, D. Chandel, H. Kaur, S. Majumdar, M. Arava, S. Gayen, Single-Cell Analysis Reveals Partial Reactivation of X Chromosome instead of Chromosome-wide Dampening in Naive Human Pluripotent Stem Cells. *Stem Cell Rep.* **14**, 745–754 (2020).

Acknowledgements: We thank members of the Reinius lab for discussions and comments on the manuscript.

Funding: This study was made possible by grants to B.R. from the Swedish Research Council (2017-01723), Åke Wiberg's Foundation, and the Ragnar Söderberg Foundation.

Author contributions: A.L.: Investigation, Methodology, Formal analysis, Conceptualization, Visualization, Data Curation, Writing - Original Draft, Writing - Review & Editing. M.E.: Resources. Q.D.: Methodology, Resources. B.R.: Investigation, Methodology, Conceptualization, Supervision, Resources, Funding acquisition, Writing - Original Draft, Writing - Review & Editing.

Competing interests: The authors declare no competing interests.

Data and materials availability: Raw Smart-seq3 data generated is publicly available at ArrayExpress accession E-MTAB-9324. Previously published raw data is available at Gene Expression Omnibus under accessions GSE45719, GSE74155, GSE109071, GSE23943 and GSE90516. Processed data and code generated during this study are available at github.com/reiniuslab/Lentini_XCU_in_vivo.

Supplementary Materials:
Materials and Methods
Figures S1-S3
Tables S1-S2
References (34-59)

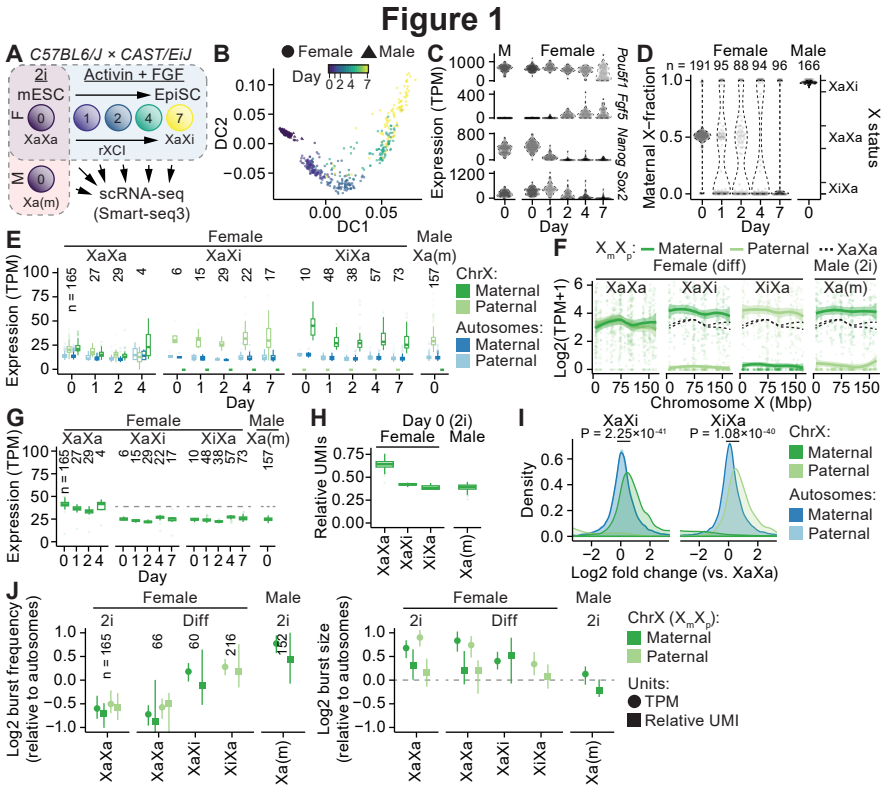

Figure 1. X-upregulation during X-inactivation establishment *in vitro*. (**A**) Schematic overview of experimental setup. (B) Diffusion map of mESC differentiation for 687 cells sequenced using Smart-seq3. (**C-D**) Expression of pluripotency and differentiation marker genes *Pou5f1*, *Fgf5*, *Nanog* and *Sox2* (C) and maternal fraction of X-chromosome expression (D) along differentiation time. (**E**) Allelic expression across differentiation days grouped by rXCI status for autosomal (n = 15,683–16,543) and X (n = 508–518) genes. (**F**) Smoothed mean (LOESS fit ± 95% confidence interval) of allelic expression across the X chromosome (n = 508–524 genes). (**G**) Same as (E) but for global expression for X genes (n = 1,158–1,337). Dashed line indicates XaXa median. (**H**) Relative UMI expression for mESCs under 2i conditions for X genes (n = 805). (**I**) Density plots of gene-wise fold changes of matching alleles between XaXa and XCI state (XaXi or XiXa; C57 and CAST allele active, respectively) in female differentiating mESCs for autosomal (n = 13,696–14,845) and X (n = 383–433) genes. Mann-Whitney *U* test P-values for active alleles. (**J**) Relative burst- frequency (left) and size (right) for active X alleles (Xa) grouped by growth condition and rXCI status. Data shown as median ± 95% confidence interval for TPM and relative UMIs for autosomal (n = 10,836–16,714) and X (n = 348–545) genes.

Figure 2

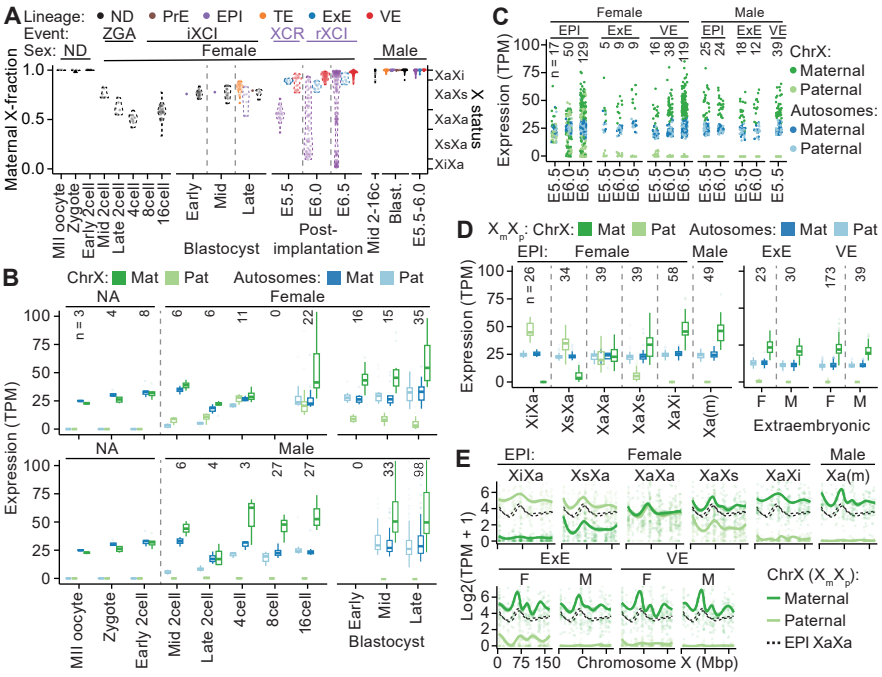

Figure 2. The dynamics of X-upregulation *in vivo*. (**A**) Maternal fraction X-chromosome expression across female mouse early embryo development with key events of X-chromosome regulation labelled above; ZGA (mid-2- to 4-cell stage), iXCI (initiating at 8- to 16-cell stage), XCR (epiblast-specific, late blastocyst to early implantation) and rXCI (epiblast-specific, following XCR). Male data shown to the right. ND = Sex not determined. (**B**) Expression levels per allele of pre-implantation development for autosomal (n = 11,164–13,347) and X (n = 323–437) genes. (**C-D**) Allelic expression of post-implantation embryos grouped by embryonic day (C) or rXCI status (D) for autosomal (n = 14,941–17,643) and X (n = 597–713). (**E**) Smoothed mean (GAM fit ± 95% confidence interval) of allelic expression across the X chromosome (genes n = 543–659), dashed lines represent EPI XaXa expression.

Figure 3

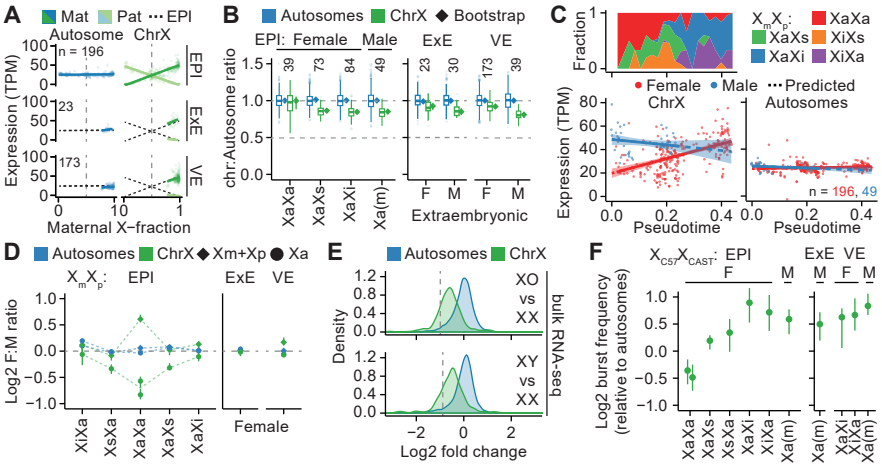

Figure 3. Linear relationship between X-upregulation and X-inactivation. (**A**) Scatter of expression level per allele and maternal X-fraction per female cell and lines indicating linear model mean ± 95% confidence interval, shown for three lineages. Dashed black lines projects EPI and dashed gray lines indicate maternal fraction 0.5. (**B**) Chromosomal expression ratios shown as box plots or bootstrapped medians (rhombus) ± 95% confidence interval. Expression-level threshold 10 TPM. F = female, M = male. (**C**) Binned X status (top) and expression of Xa allele shown as linear model mean ± 95% confidence interval for autosomal (n = 17,643) and X (n = 713) genes (bottom) along pseudotime trajectory in EPI cells. Dashed lines represent values predicted from linear model. (**D**) Female:male ratios for the active X allele (Xa; circles) or global expression (Xm+Xp; rhombus) shown as median and ± 95% confidence interval. (**E**) Density plot of differential expression in mESC bulk RNA-seq data (XO n = 2, XX n = 12, XY n = 14) for autosomal (n = 10,961) and X (n = 405) genes. Dashed line indicates expected half of autosomal expression. (**F**) Burst frequencies of the Xa allele (n = 252–316 genes) relative to autosomal alleles of same strain (n = 9,204–10,577 genes), shown as median and 95% confidence interval. (**A-B, D**) Autosomal (n = 14,941–17,643) and X (n = 597–713) genes.

Figure 4

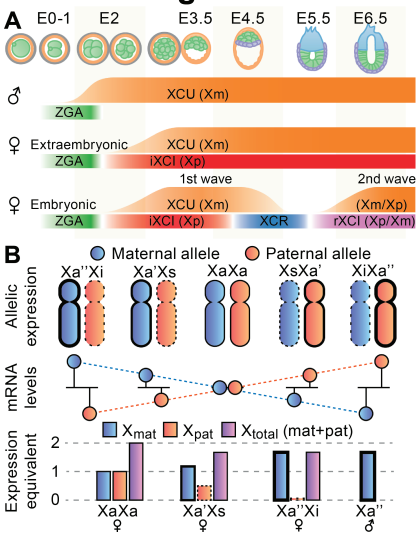

Figure 4. Model of X-upregulation. (**A**) Schematic of sex- and lineage-specific dynamics of X-upregulation (XCU) across mouse embryonic development. (**B**) Proposed model of XCU as a flexible mechanism of allelic dosage balancing. As one allele is gradually silenced, the concentration of available transcription factors is shifted towards the active allele (Xa), increasing transcriptional burst frequencies and mRNA levels in a linear fashion. However, the single hyperactive allele (Xa") does not fully reach the combined expression level of two moderately active alleles in XaXa state.